

Provided for non-commercial research and education use.
Not for reproduction, distribution or commercial use.



This article appeared in a journal published by Elsevier. The attached copy is furnished to the author for internal non-commercial research and education use, including for instruction at the authors institution and sharing with colleagues.

Other uses, including reproduction and distribution, or selling or licensing copies, or posting to personal, institutional or third party websites are prohibited.

In most cases authors are permitted to post their version of the article (e.g. in Word or Tex form) to their personal website or institutional repository. Authors requiring further information regarding Elsevier's archiving and manuscript policies are encouraged to visit:

<http://www.elsevier.com/copyright>



Contents lists available at ScienceDirect

Earth and Planetary Science Letters

journal homepage: www.elsevier.com/locate/epsl

Conditions required for oceanic anoxia/euxinia: Constraints from a one-dimensional ocean biogeochemical cycle model

Kazumi Ozaki^{*}, Shigeo Tajima¹, Eiichi Tajika²

Department of Earth and Planetary Science, School of Science, University of Tokyo, 7-3-1, Hongo, Bunkyo-ku, Tokyo 113-0033, Japan

ARTICLE INFO

Article history:

Received 28 July 2010

Received in revised form 7 January 2011

Accepted 6 February 2011

Available online 3 March 2011

Editor: P. DeMenocal

Keywords:

anoxia

euxinia

oceanic anoxic events

biogeochemical cycles

phosphorus cycle

ABSTRACT

Widespread black shale depositional intervals termed oceanic anoxic events (OAEs) occurred repeatedly during the Phanerozoic Eon. Here we developed a new vertical one-dimensional ocean biogeochemical cycle model that involves several chemical reactions in an oxic–anoxic–sulfidic water column. To explore the theoretical constraints for global oceanic anoxia/euxinia quantitatively and systematically, we conducted sensitivity analyses of the proposed causal mechanisms, including elevated rates of riverine phosphorus (P) input, ocean stagnation, and lowered oxygen solubility due to climate warming. We gave special attention to the vertical chemical structure of the ocean and also to the characteristic behaviors of the marine P cycle under anoxic conditions, because the relationship between the depth of anoxia and the benthic phosphorus flux could be important for the occurrence of oceanic anoxia/euxinia. Steady-state simulations indicated that (1) a decrease in ocean stagnation or oxygen solubility is not enough by itself to achieve widespread anoxia with the present reactive P river input rate, and (2) shallow water anoxia followed by massive P liberation from surface sediments can lead to widespread eutrophication and anoxia/euxinia. We conclude that elevated riverine flux of reactive P is the most important factor for triggering global anoxic events via a positive feedback loop among ocean anoxia, phosphorus regeneration, and surface biological productivity.

© 2011 Elsevier B.V. All rights reserved.

1. Introduction

The formation of organic-rich, laminated sediments termed black shale occurred sporadically during the Phanerozoic. Since they are usually interpreted as a product of anoxic/euxinic bottom water conditions, such depositional events are called oceanic anoxic events (OAEs) (e.g., Schlanger and Jenkyns, 1976). Over the past three decades, many studies have investigated the connections among enhanced organic carbon (C_{org}) burial, ocean anoxia, biological extinction, and climate change (e.g., Arthur and Sageman, 1994; Jenkyns, 2010 and references therein). Accumulation of black shale accompanied by anomalous carbon isotopic excursions must indicate rapid and drastic disturbances in carbon cycling in the atmosphere–ocean system.

The proposed mechanisms for widespread, prolonged ($<10^6$ yr) oxygen depletion events are divided into two principal types: (1) enhanced biological productivity in the surface ocean, resulting

in the consumption of large amounts of dissolved oxygen in intermediate to deep water (e.g., Hochuli et al., 1999; Kuypers et al., 2002; Schlanger and Jenkyns, 1976) and (2) ocean stagnation, which prevents oxygen from reaching deep water (e.g., Bralower and Thierstein, 1984; Erbacher et al., 2001; Hotinski et al., 2001). Considering the frequent occurrence of OAEs in the greenhouse world, a decrease in oxygen solubility into seawater owing to warm climate conditions would be an additional factor affecting the conditions required for global oxygen depletion in the ocean (e.g., Hotinski et al., 2001; Meyer and Kump, 2008). Furthermore, Bjerrum et al. (2006) obtained results suggesting that a larger shelf area acts as a buffer against oceanic eutrophication, resulting in lower productivity and an oxygenated ocean. They argued that a high sea-level stand reduces the organic carbon burial rate, suggesting a positive feedback loop between global warming and sea-level rise.

Studies of the early diagenetic processes at the sediment–water interface have revealed that the sediment retention potential for phosphorus tends to be depressed under anoxic bottom water conditions (e.g., Ingall and Jahnke, 1994; Ingall et al., 1993; Van Cappellen and Ingall, 1994). Observations of modern anoxic marine sediments revealed that the molar ratio of buried C_{org} to $P_{reactive}$ is almost 200 under fully anoxic–sulfidic conditions, whereas it is almost 60 or less in fully oxic settings (Algeo and Ingall, 2007), where $P_{reactive}$ represents the total bio-available phosphorus, including the organic (P_{org}), iron-bonded (P_{Fe}), and authigenic (P_{auth}) phases, i.e., $P_{reactive} \equiv P_{org} + P_{Fe} + P_{auth}$ (Anderson et al., 2001). Several recent

^{*} Corresponding author. Tel.: +81 3 5841 4250.

E-mail address: ozaki@eps.s.u-tokyo.ac.jp (K. Ozaki).

¹ Present address: Microdevice Operations Division, Imaging IF Business Unit, Seiko Epson Corporation, Fujimi Plant 281 Fujimi, Fujimi-machi, Suwa-gun, Nagano-ken, 399-0293, Japan.

² Present address: Department of Complexity Science and Engineering, Graduate School of Frontier Sciences, The University of Tokyo, 5-1-5, Kashiwanoha, Kashiwa-shi, Chiba-ken, 277-8561, Japan.

studies have reported decreases in the total phosphorus accumulation rate and increases in the C_{org}/P_{total} ratio during OAEs (Kraal et al., 2010; Mort et al., 2007, 2008; Murphy et al., 2000; Nederbragt et al., 2004). The intrinsic positive feedback loop among oxygen depletion, phosphorus regeneration, and surface biological productivity could promote and sustain anoxia during OAEs. Because of this feedback process, it is possible for the stagnant ocean to have a highly productive anoxic environment (Ingall and Jahnke, 1994; Van Cappellen and Ingall, 1994). The surface biological productivity is limited by the supply of P via upwelling of nutrient-rich intermediate waters to the surface ocean. However, on timescales longer than the residence time of P in the ocean ($>10^4$ years), the surface productivity is limited by the P inventory in the intermediate ocean, which is limited not only by the riverine P supply from continents to the ocean but also by the recycling of phosphorus in the ocean. Hence, this feedback process could be critical. This process may also increase the atmospheric oxygen levels (pO_2) through the accumulation of large amounts of organic carbon during OAEs, ultimately resulting in ocean oxygenation (Handoh and Lenton, 2003; Mort et al., 2007, 2008; Tsandev and Slomp, 2009; Van Cappellen and Ingall, 1996).

Although these suggestions for linkages among biogeochemical processes during OAEs are intriguing, few studies have quantitatively and systematically examined the effects of these causal mechanisms on widespread oceanic anoxia (Bjerrum et al., 2006; Hotinski et al., 2000; Meyer et al., 2008; Sarmiento et al., 1988; Shaffer, 1989; Tsandev and Slomp, 2009). In this article, we investigate the conditions for the occurrence of oceanic anoxia/euxinia by using a new ocean biogeochemical cycle model to reconstruct the marine biochemical cycling of carbon, alkalinity, nitrogen, oxygen, phosphorus, and sulfur. Because dissolved inorganic matter in the ocean shows remarkable vertical structure features, we develop a one-dimensional vertical ocean biogeochemical model. We evaluate the contributions of the causal mechanisms and describe a scenario for the occurrence of OAEs based on the behaviors of redox-dependent marine biogeochemical cycles.

2. Model description

2.1. Model ocean configuration and basic equation

We developed a vertical one-dimensional ocean biogeochemical model that includes ocean circulation (advection); vertical diffusion; horizontal water exchange; biological pumps of organic matter and carbonate; dissolution, decomposition, sedimentation, and burial of

biogenic particles; and several redox reactions in aerobic and anaerobic environments. We also considered the input of material from external reservoirs to the ocean (as the sum of riverine input and deposition from the atmosphere) and carbon isotope fractionation. We considered the total dissolved inorganic carbon (DIC), $\delta^{13}C$ of DIC, total alkalinity (Alk), oxygen (O_2), phosphate (PO_4), nitrate (NO_3), ammonium (NH_4), sulfate (SO_4), and hydrogen sulfide (H_2S) as dissolved chemical components of seawater.

The model ocean consists of a surface mixed layer (M), a high-latitude surface layer (H), a deepwater circulation box (DCB), and multiple layers of ocean interior (O; see Fig. 1a). Below the surface layers (M and H), we used an averaged modern ocean topography (Millero, 2006) and assumed a deepest ocean depth of 6100 m, the area of which is less than 5% of the entire sea surface area (Fig. 1b). The ocean interior is divided into 60 depth levels with a 100-m vertical grid spacing; the layers are labeled with j ($j=1 \dots 60$) from surface to bottom (Fig. 1a). This treatment allows us to calculate the amount of buried biogenic particles in seafloor sediments at each depth. We assumed downwelling of the surface waters at H to the DCB and flows into the intermediate to deep oceanic layers, which, in turn, provide upwelling water to M.

The concentration of dissolved component X in the aphotic zone changes with time, as follows:

$$\frac{\partial[X]}{\partial t} = -A(z)w(z)\frac{\partial[X]}{\partial z} + \frac{\partial}{\partial z}\left(A(z)K(z)\frac{\partial[X]}{\partial z}\right) + B + \mathcal{R} + \mathcal{D}. \quad (1)$$

$[X]$ represents the concentration of dissolved component X , and z represents the water depth (increasing upward). The first and second terms on the right-hand side express the advection and diffusion components, respectively. The factors $K(z)$, $A(z)$, and $w(z)$ are the vertical diffusion coefficient, areal fraction of the water layer at depth z to the sea surface area of $3.62 \times 10^{14} \text{ m}^2$, and upwelling rate. The factors B , \mathcal{R} , and \mathcal{D} represent internal sources and sinks resulting from biological processes, chemical processes (formulated in the following subsections), and the lateral inflow of downwelling water, respectively. In this model, DCB water is assumed to flow into each ocean layer ($z < -1100 \text{ m}$) in proportion to the volume of the layer. The oxygen concentration in the surface water is restored to a saturated concentration calculated by using the oxygen solubility in seawater at a given temperature (288 K for M, 275 K for H) and salinity (35 psu for M and 34 psu for H) and an atmospheric oxygen concentration of 0.21 atm (Garcia and Gordon, 1992). The upwelling rate is assumed to depend on the water depth owing to the seafloor topography and the route of deepwater lateral inflow. To include the highly convective

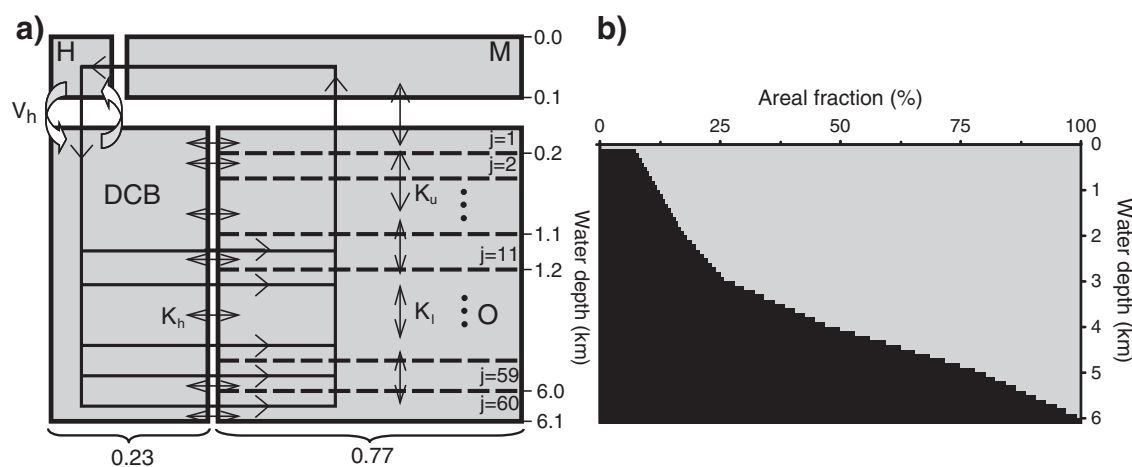


Fig. 1. (a) Schematic illustration of the model ocean used in this study. “M,” “H,” and “DCB” denote the mixed surface layer, high-latitude surface layer, and deepwater circulation box, respectively. An ocean area of 5% is assumed for the high-latitude surface box. The area of the DCB is held at 23%. K_u , K_l , K_h , and V_h are the high vertical diffusion coefficient, low vertical diffusion coefficient, horizontal diffusion coefficient, and polar convection, respectively. (b) Seafloor topography assumed in this study.

Ekman layer in the upper part of the ocean, we adopted a higher value for the vertical diffusion coefficient in the uppermost 500 m of the ocean (5000 m²/yr for $z > -500$ m, 2500 m²/yr for $z < -500$ m; Ikeda and Tajika, 2002; Ikeda et al., 2002). We also included high-latitude convection between H and the DCB (57.4 Sv; 1 Sv = 10⁶ m³/s) and horizontal diffusion between the DCB and the aphotic zones ($K_h = 0.001$ l/yr for $z > -500$ m, $K_h = 3 \times 10^{-5}$ l/yr for $z < -500$ m). Previous studies have applied similar mathematical treatments (e.g., Misumi et al., 2009; Shaffer and Sarmiento, 1995).

2.2. Biological pump

Production of particulate organic matter (POM) and carbonate is assumed to occur only within a 100-m-thick surface layer (M and H). Because the supply of phosphate to the surface water ultimately limits the net primary production on geological timescales (e.g., Broecker and Peng, 1982; Tyrell, 1999), we assumed that export production of biogenic particles from the surface layer (M) is determined by the budget of phosphate supplied to M (which is dominated by diffusive transport from deep water). Export production at high latitudes tends to be limited mainly by a combination of incident solar radiation, mixed layer thickness, iron availability, and ice formation rather than by phosphate availability. Therefore, we assumed that the efficiency of biogenic production is lower at high latitudes (e.g., Knox and McElroy, 1984; Lenton, 2000), and that downwelling waters contain a certain level of nutrients (preformed nutrients). The export production of carbonate is calculated from those of POM in both high and moderate latitude regions with a constant ratio of carbonate to organic carbon rain of 0.08 (Yamanaka and Tajika, 1996). We assumed that DCB waters are oversaturated with respect to carbonates (both calcite and aragonite), as seen in the north Atlantic today. Hence, all carbonates entering the DCB are buried without dissolution.

For the elemental composition of POM, we assumed the traditional Redfield ratio of C:N:P = 106:16:1 (Redfield et al., 1963). We also assumed that this ratio does not change during downward transport through the water column (Anderson and Sarmiento, 1994; Delaney, 1998). We assumed 100 m/day for the settling speed of biogenic particles (e.g., Suess, 1980) for simplicity, although a very wide range of values has been reported (e.g., Berelson, 2002).

2.3. Redox reactions and kinetics

We employed the multi-G method to treat POM decomposition in the water column. We classify POM into three components ($G_1 = 68\%$, $G_2 = 31\%$, $G_3 = 1\%$ in weight) having different rate constants ($k_1 = 60\%/day$ for G_1 , $k_2 = 10\%/day$ for G_2 , $k_3 = 0\%/day$ for G_3). We

chose these values on the basis of consistency with the typical profile of the POM sinking flux estimated from present-day sediment trap studies.

We consider biogeochemical cycles under both oxic and anoxic ocean conditions (Table 1). In an oxic water column, organic matter is remineralized by an aerobic oxidation process (Eq. (2)). In the absence of oxygen, however, heterotrophic denitrification (Eq. (3)) and sulfate reduction (Eq. (4)) will occur (e.g., Froelich et al., 1979; Shaffer, 1989). In Table 1, α (= 106) and β (= 16) are the ratios for carbon and nitrogen to phosphorus, respectively, in POM. The decomposition rates of component G_i ($i = 1, 2, 3$) for each POM oxidation process in the j th water layer are written as Eqs. (7)–(9), where K and K' are the saturation constant and half-saturation constant, respectively. The oxidants for organic matter decomposition change gradually, depending on the amount of each oxidant. These Monod-type expressions are most widely used in mathematical models of POM oxidation processes (e.g., Boudreau, 1996). The parameter values are adopted from previous studies of early diagenetic processes in marine sediments (Boudreau, 1996; Van Cappellen and Wang, 1996). Although recent studies argued that the sulfate concentration during the Cretaceous was relatively low (Wortmann and Chernyavsky, 2007) and may be disturbed by submarine volcano activity (Adams et al., 2010), sulfate was a major component of the Phanerozoic oceans and has been an important oxidizing agent in anaerobic systems. We therefore assume that the saturation constant K_{SO_4} can be set to zero in this study.

Ammonium and hydrogen sulfide are produced via POM decomposition, and oxidation reactions of these molecules (nitrification and sulfide oxidation; Eqs. (5) and (6), respectively) will occur under aerobic conditions (Table 1). The kinetic expressions are assumed to be a first-order rate process with respect to each of the individual concentrations (Eqs. (10) and (11)). Here, k_{NH_4} and k_{H_2S} are the rate constants of each oxidation process (Table 1). We adopted these values from a numerical study of the suboxic layer of the Black Sea, which is the largest anoxic/euxinic basin on the present-day Earth (Oguz et al., 2001).

2.4. Burial of organic carbon and phosphorus

To evaluate the C_{org} burial rate at each depth, we used the relationship between the burial efficiency of sedimentary organic carbon (BE) and the sedimentation rate (SR , in cm/yr) demonstrated by Henrichs and Reeburgh (1987):

$$BE(z) = SR(z)^{0.4} / 2.1. \quad (2)$$

Table 1
Redox reactions included in this model.

Redox reactions	Formulae	Constants
Aerobic oxidation of POM: $(CH_2O)_\alpha(NH_3)_\beta(H_2PO_4) + \alpha O_2 + \beta H^+ \rightarrow \alpha CO_2 + \beta NH_4^+ + H_2PO_4^- + H^+ + \alpha H_2O$ (2)	$r_{ij}^{O_2} = k_{ij}^{O_2} \frac{[O_2]_j}{K_{O_2} + [O_2]_j}$ (7)	$K_{O_2} = K'_{O_2} = 8 \times 10^{-3} \text{ mol/m}^3$
Denitrification: $(CH_2O)_\alpha(NH_3)_\beta(H_2PO_4) + \frac{4}{5} \alpha NO_3^- + \left(\frac{4}{5} \alpha + \beta\right) H^+ \rightarrow \alpha CO_2 + \beta NH_4^+ + \frac{2}{5} \alpha N_2 + H_2PO_4^- + H^+ + \frac{7}{5} \alpha H_2O$ (3)	$r_{ij}^{NO_3} = k_{ij}^{NO_3} \frac{K'_{O_2} \frac{[NO_3]_j}{K_{NO_3} + [NO_3]_j}}{K_{O_2} + [O_2]_j}$ (8)	$K_{NO_3} = K'_{NO_3} = 3 \times 10^{-2} \text{ mol/m}^3$
Sulfate reduction: $(CH_2O)_\alpha(NH_3)_\beta(H_2PO_4) + \frac{4}{5} \alpha NO_3^- + \left(\frac{4}{5} \alpha + \beta\right) H^+ \rightarrow \alpha CO_2 + \beta NH_4^+ + \frac{2}{5} \alpha N_2 + H_2PO_4^- + H^+ + \frac{7}{5} \alpha H_2O$ (4)	$r_{ij}^{SO_4} = k_{ij}^{SO_4} \frac{K'_{O_2} \frac{K'_{NO_3} \frac{[SO_4]_j}{K_{SO_4} + [SO_4]_j}}{K_{NO_3} + [NO_3]_j}}{K_{O_2} + [O_2]_j}$ (9)	$K_{SO_4} = 0.0 \text{ mol/m}^3$
Nitrification: $NH_4^+ + 2O_2 + 2HCO_3^- \rightarrow NO_3^- + 2CO_2 + 3H_2O$ (5)	$\mathcal{R}_{NH_4} = k_{NH_4} [NH_4][O_2]$ (10)	$k_{NH_4} = 18,250 \text{ (mol/m}^3\text{)}^{-1} \text{ yr}^{-1}$
Sulfide oxidation: $H_2S + 2O_2 + 2CO_3^{2-} \rightarrow SO_4^{2-} + 2HCO_3^-$ (6)	$\mathcal{R}_{H_2S} = k_{H_2S} [H_2S][O_2]$ (11)	$k_{H_2S} = 3650 \text{ (mol/m}^3\text{)}^{-1} \text{ yr}^{-1}$

Because the sedimentation rate depends strongly on the water depth in the ocean, we applied the relationship between water depth z (m) and sedimentation rate SR shown by Tromp et al. (1995):

$$z = 2700 \cdot \operatorname{erfc}(2.1 + \log SR). \quad (3)$$

Using these formulas with the sea floor topography and C_{org} depositional flux, we can calculate the C_{org} burial rate in each sediment underlying the j th water layer (B_j^{Corg}). We found that 1.39% of C_{org} exported from the euphotic zone is ultimately buried, and almost 79% of the total C_{org} burial is accounted for by the sediments on the shallowest part of the seafloor ($j=1$) at a water depth of 200 m.

Phosphorus is an essential nutrient for living organisms in the ocean. Therefore, its availability is one of the dominant factors limiting the productivity of the surface ocean. The marine carbon and phosphorus cycles are linked not only by the C/P ratio of POM but also through the $C_{\text{org}}/P_{\text{reactive}}$ ratio in marine sediments. In other words, marine biological productivity on short timescales is greatly affected not by the riverine P input flux but by the efficiency of P recycling in the oceans (Van Cappellen and Ingall, 1994). In fact, the estimated P diffusive flux from seafloor sediments is much greater than the riverine P flux (Delaney, 1998; Hensen et al., 1998; Ruttnerberg, 2003; Wallmann, 2003). Preferential regeneration of P relative to C has been reported for several modern anoxic environments (e.g., Algeo and Ingall, 2007; Anderson et al., 2001; Filippelli, 2001; Ingall and Jahnke, 1997), indicating that the efficiency of sedimentary reactive P burial is depressed under anoxic condition. On the basis of sedimentary core records, evidence for decreases in phosphorus accumulation and increases in the $C_{\text{org}}/P_{\text{reactive}}$ ratio during OAEs has also been reported (Ingall et al., 1993; Kraal et al., 2010; Mort et al., 2007, 2008; Murphy et al., 2000; Nederbragt et al., 2004). Therefore, it is very important to examine the phosphorus diffusive flux at the sediment–water interface under oxygen-depleted environments for quantitative discussion of marine biogeochemistry during oceanic anoxia.

Most of the dissolved P derived from organic matter degradation through early diagenesis diffuses out of sediment, but the remainder is ultimately buried as P bonded onto iron oxyhydroxides or authigenic phosphate minerals (e.g., Filippelli, 2001; Ruttnerberg, 2003; Ruttnerberg and Berner, 1993). Under fully oxic conditions, we assume that P_{org} , P_{Fe} , and P_{auth} account for 25%, 25%, and 50%, respectively, of the total reactive P buried in sediment (Ruttnerberg, 1993). Some studies have attempted to formulate the P_{reactive} burial rate by adapting empirical methods in which the rate is controlled by the oxygen concentration in deep water (Lenton and Watson, 2000; Slomp and Van Cappellen, 2007; Van Cappellen and Ingall, 1994). On the basis of previous studies (Slomp and Van Cappellen, 2007; Van Cappellen and Ingall, 1994, 1996), we assume the following formulation for the $C_{\text{org}}/P_{\text{org}}$ ratio of the buried organic phase:

$$(C/P)_j = \begin{cases} (C/P)^0 \cdot \frac{1 + \exp(-0.001/SR_j)}{2} & \text{for } [O_2]_j > [O_2]^* \\ \frac{(C/P)^0 \cdot (C/P)^a}{\frac{[O_2]_j}{[O_2]^*} \cdot (C/P)^a + \left(1 - \frac{[O_2]_j}{[O_2]^*}\right) \cdot (C/P)^0} \cdot \frac{1 + \exp(-0.001/SR_j)}{2} & \text{for } [O_2]_j < [O_2]^* \end{cases} \quad (4)$$

In the above equations, $[O_2]_j$ represents the oxygen concentration of the j th water layer, and SR_j represents the sedimentation rate in sediments underlying the j th water layer (in cm/yr). The term including an exponential represents the dependence of the buried C/P organic ratio to SR_j . In the pelagic deep ocean, preferential P regeneration is not observed owing to the long timescale of diagenesis until burial (Ingall and Van Cappellen, 1990). We adopted $[O_2]^* = 0.25 \text{ mol/m}^3$. $(C/P)^0$ is set to twice the value of the Redfield ratio (106), and $(C/P)^a$ is an upper limit assumed for sedimentary

organic matter buried under fully anoxic overlying waters, estimated as 10 times larger than the Redfield value on the basis of studies of various modern anoxic basin sediments (e.g., Slomp and Van Cappellen, 2007). The burial rate of P_{org} in sediments underlying the j th water layer (B_j^{Porg}) is calculated as the C_{org} burial rate (B_j^{Corg}) divided by $(C/P)_j$.

Under oxic bottom water conditions, remineralized organic phosphorus can be trapped well at the sediment–water interface. In contrast, under anoxic bottom water conditions, a lack of ferric iron phases allows most remineralized P to diffuse out of the sediment (e.g., Ruttnerberg, 2003). This redox-dependent P burial flux is represented as

$$B_j^{\text{PFe}} = \begin{cases} \frac{B_j^{\text{Corg}}}{(C/P)_j} \equiv B_j^{\text{PFe,oxic}} & \text{for } [O_2]_j \geq [O_2]^* \\ B_j^{\text{PFe,oxic}} \times \frac{[O_2]_j}{[O_2]^*} & \text{for } [O_2]_j < [O_2]^* \end{cases}, \quad (5)$$

where B_j^{PFe} is the burial rate of phosphorus owing to adsorption onto iron hydroxide in marine sediments underlying the j th water layer. We assumed that this rate is linearly proportional to the oxygen concentration (Slomp and Van Cappellen, 2007). Note that B_j^{PFe} equals B_j^{Porg} when $[O_2]_j \geq [O_2]^*$.

Some have also proposed that authigenic phosphorus burial, a dominant process for phosphorus burial today (e.g., Ruttnerberg, 1993), depends on the redox condition of the bottom water (Slomp and Van Cappellen, 2007; Slomp et al., 2002). However, studies of Mediterranean sapropels (Slomp et al., 2002) suggest that this mechanism tends to be less effective under anoxic conditions. We adopt the following formulation for this, with the redox dependence used by Slomp and Van Cappellen (2007):

$$B_j^{\text{Pauth}} = \begin{cases} 2 \times B_j^{\text{PFe,oxic}} & \text{for } [O_2]_j \geq [O_2]^* \\ 2 \times B_j^{\text{PFe,oxic}} \times \left(0.5 + 0.5 \frac{[O_2]_j}{[O_2]^*}\right) & \text{for } [O_2]_j < [O_2]^* \end{cases}. \quad (6)$$

Reactive P settles at the oceanic sediment–water interface as a form of POM. Most is decomposed in the sediments and diffused to the bottom water. Part of the liberated P is trapped by iron hydroxides or buried as authigenic minerals. If the above formulations are adopted, the ratio $\langle C_{\text{org}}/P_{\text{reactive}} \rangle$ (= total organic carbon burial rate/total reactive phosphorus burial rate in the ocean) varies between 54 and 174 as a function of the ocean's redox state. This is in the range of an estimation derived from various observations of modern/ancient sediments (Algeo and Ingall, 2007).

The equations were solved numerically with the finite difference method. The model includes physical, chemical, and biological processes in the oceans. The characteristic timescales of these processes encompass a wide range. In particular, that of chemical reactions is significantly shorter than those of the other processes. Chemical reactions are therefore treated implicitly to maintain the stability of the solution. The equations are integrated for a sufficiently long time until the system approaches its steady state. All the results discussed below represent the steady state.

3. Results and discussion

3.1. Standard case

First, we show the results of the standard case for this model, which mimics the pre-anthropogenic ocean environment. In this case, we assume an ocean circulation rate of 20 Sv and a riverine reactive P input flux of 0.18 Tmol P/yr (Tmol = 10^{12} mol). The obtained vertical profiles of the dissolved oxygen and phosphate concentrations are

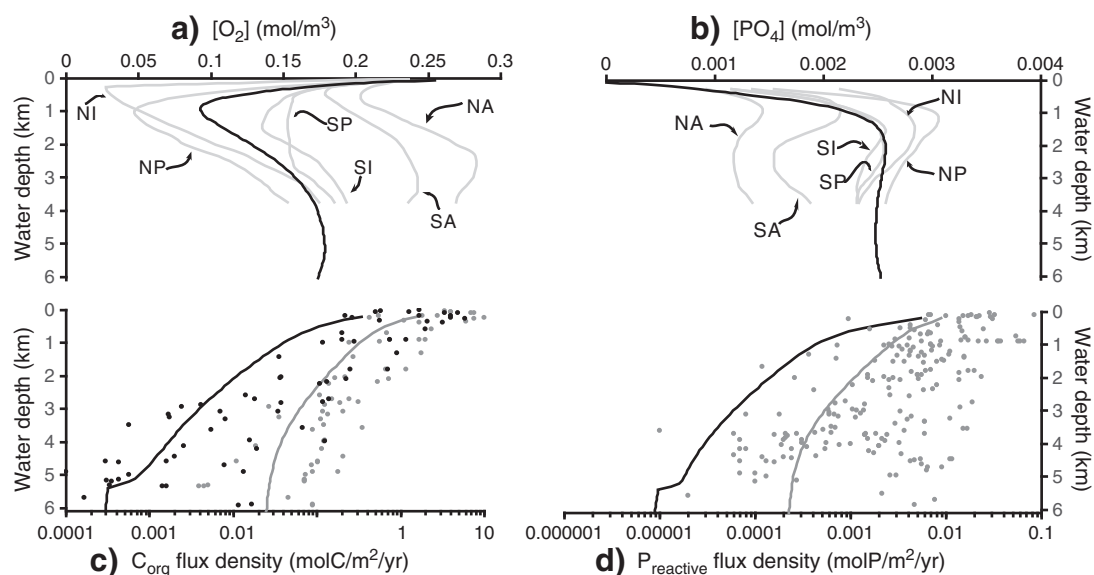


Fig. 2. Vertical profiles of (a) dissolved oxygen and (b) phosphate in the standard case (riverine input flux of reactive P, 0.18 Tmol P/yr; ocean circulation rate, 20 Sv). Vertical profiles obtained from GEOSECS data are also shown (Shaffer, 1996; unit conversion from mol/kg to mol/m³ using global averaged density profile). Abbreviations: NA = North Atlantic, SA = South Atlantic, NI = North India, NP = North Pacific, SP = South Pacific. (c) Vertical profiles of C_{org} depositional (gray curve) and burial flux (black curve) densities for the standard case. Field data on depositional flux (gray circles) and burial flux (black circles) from Betts and Holland (1991) are also shown. (d) Vertical profiles of benthic flux (gray curve) and burial flux (black curve) densities of $P_{reactive}$ for the standard case. Field data on phosphorus benthic flux (Hensen et al., 1998; McManus et al., 1997) are also shown (gray circles). Observational data having negative value are excluded.

shown in Fig. 2a and b, respectively (solid black curves). Vertical profiles of the dissolved oxygen and phosphate concentrations obtained from GEOSECS data for the North and South Atlantic, Pacific, and Indian oceans (Shaffer, 1996) are also shown. In the standard case, the total export production and total burial rate of C_{org} are 795 and 11 Tmol C/yr, respectively. The inventories of phosphate and nitrate are 2.92×10^{15} mol P and 42.32×10^{15} mol N, respectively. The phosphorus residence time is 16.2 kyr, which is somewhat small but consistent with recent estimates of 20 kyr or shorter (Benitez-Nelson, 2000; Ruttenberg, 2003). The depositional and burial flux densities of C_{org} in the sediments are illustrated in Fig. 2c. The benthic and burial flux densities of $P_{reactive}$ in the sediments are illustrated in Fig. 2d. Observational data points (Betts and Holland, 1991; Hensen et al., 1998; McManus et al., 1997) are also plotted. Thus, our standard results can reproduce the characteristic features of oceanic chemical structures, although we do not claim a perfect fit to field data.

3.2. Sensitivity to reactive P riverine input flux and ocean circulation rate

We examine the response of the ocean environment to changes in riverine P input flux and ocean circulation rate, which have been proposed as principal factors causing global oceanic anoxia. The left column of Fig. 3 shows the sensitivity to the riverine P input flux (R_p) with a standard ocean circulation rate of 20 Sv. Black and white lines in Fig. 3a represent the contours of the dissolved oxygen and hydrogen sulfide concentrations, respectively. In the steady state, enhanced delivery of P from continents leads to eutrophication of the ocean, resulting in high surface productivity. As R_p increases, anoxia ($[O_2] < 0.001$ mol/m³) appears at intermediate depths owing to expansion of the oxygen minimum zone. As a result, ammonium and hydrogen sulfide build up in that region (Fig. 3a, c). Here, we define intermediate water anoxia (IWA) as the existence of oxygen-depleted water at intermediate depths while the deep water is oxygenated. In contrast, we also define deepwater anoxia (DWA) as the expansion of anoxia to the ocean bottom. We also define OXIC as fully oxic conditions. In the sensitivity analysis described above, IWA appears for $R_p/R_p^* = 1.4$ –1.9 (R_p^* is the standard value of 0.18 Tmol P/yr), and DWA appears for $R_p/R_p^* > 1.9$.

In fully oxic oceans, the $[NO_3]/[PO_4]$ ratio at each water depth remains close to the Redfield ratio. However, deviation occurs in the anoxic water column owing to denitrification, which depletes nitrate via N_2 degassing (Fig. 3c). Thus, the anoxic ocean tends to lose fixed nitrogen. Nitrogen depletion is assumed to be compensated by the supply of nitrogen from the atmosphere. In fact, biomarker studies of Cretaceous black shale have indicated that nitrogen fixers became the primary producers during OAEs (Junium and Arthur, 2007; Kashiyama et al., 2008; Kuypers et al., 2004; Ohkouchi et al., 2006).

As R_p increases, hydrogen sulfide builds up in the anoxic intermediate depth and then develops in deep water. For $R_p/R_p^* = 2.05$ –2.15, euxinic conditions ($[H_2S] > 0.1$ mol/m³) appear at intermediate depths. On the basis of the hydrogen sulfide profiles, we classify the oceanic redox conditions into non-sulfidic, intermediate water euxinia (IWE), and deepwater euxinia (DWE). As the riverine P input flux increases, the oceanic redox condition changes from OXIC/non-sulfidic to DWA/DWE; at the same time, phosphate and reductants (such as ammonium and hydrogen sulfide) accumulate in the deep oceans (Fig. 3a, c). In Fig. 3, anoxic and euxinic water conditions are represented by light and dark shading.

The oceanic redox condition changes dramatically around $R_p/R_p^* = 2.2$ (Fig. 3). This is because of a massive P flux from sediments to the bottom water on continental shelves, where almost 80% of the exported organic matter is buried. Shallow water anoxia strongly promotes a positive feedback mechanism through eutrophication, enhancement of biological productivity, and anoxia.

Sluggish ocean circulation may not strongly control the redox conditions in the ocean's interior, as seen on the right side of Fig. 3. Anoxia appears only when the ocean circulation rate is very slow (<5 Sv), and euxinia does not appear even when the ocean is completely stagnant with the standard P input rate. This is because the phosphorus flux from sediment to bottom water deduced by deepwater anoxia has a relatively weak effect on the overall oceanic redox conditions. These results suggest that it is important to consider the locations of anoxia and phosphorus benthic flux in paleoceanographic studies.

From the above results, we conclude that the riverine P input flux might be an important causal mechanism for the occurrence of global oceanic anoxia/euxinia, and ocean stagnation cannot be a major

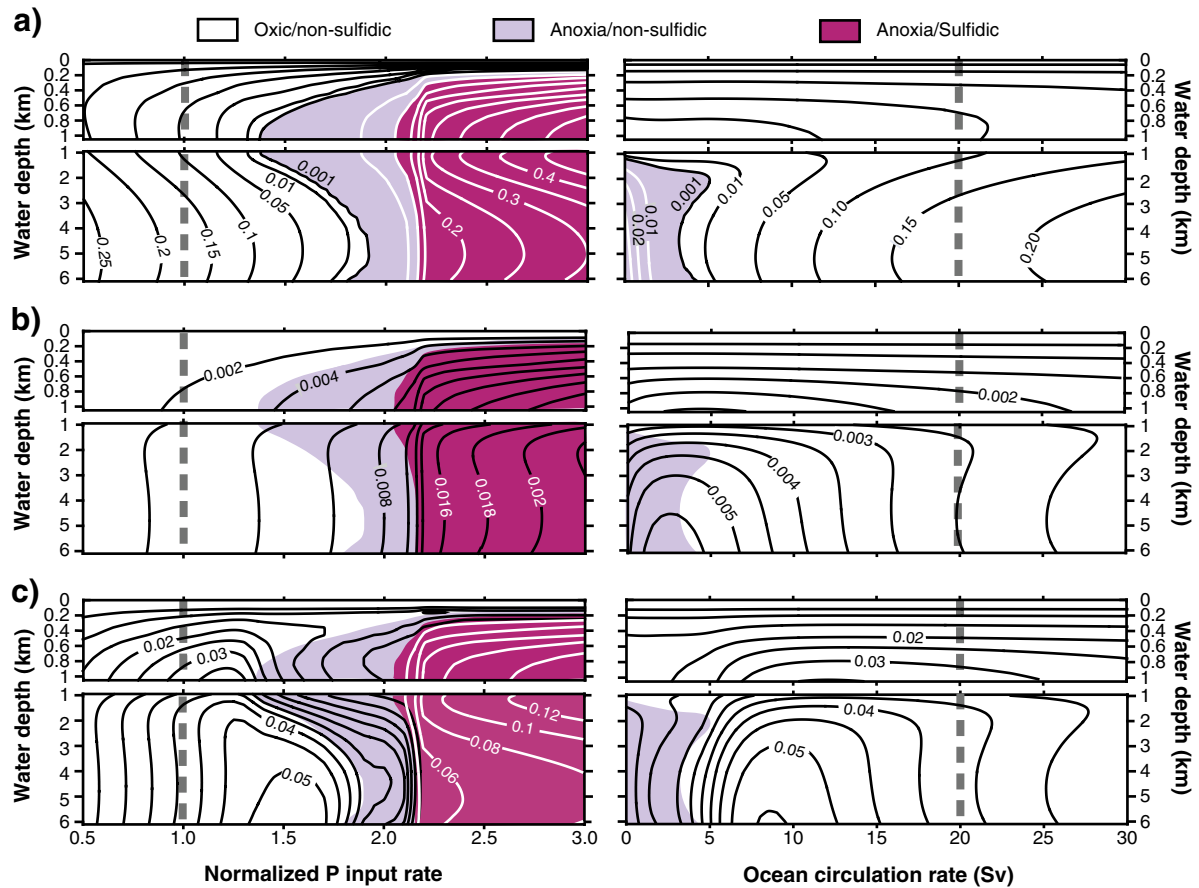


Fig. 3. Effect of riverine P input flux and ocean circulation rate on the vertical profiles of (a) oxygen (black curves) and hydrogen sulfide (white curves), (b) phosphate, and (c) nitrate (black curves) and ammonium (white curves) concentrations (in mol/m³). Anoxic water ([O₂] < 0.001 mol/m³) and euxinic water ([H₂S] > 0.1 mol/m³) are represented by light and dark shading, respectively.

causative factor for anoxic events without additional causal mechanisms. In this study, we did not distinguish explicitly between the coastal region and open ocean. A study with a model that considered the coastal region separately indicated that the productivity of the pelagic ocean decreases as the ocean ventilation weakens, while that of the coastal region increases, promoting coastal anoxia (Slomp and Van Cappellen, 2007). As shown in this study, however, an enhanced riverine P input flux causes anoxia in the coastal region much more effectively via enhancement of productivity, whereas sluggish ocean conditions promote anoxia at depth.

3.3. Conditions for occurrence of oceanic anoxia/euxinia

For further systematic examination of the effect of riverine P input flux and the ocean circulation rate on oceanic redox conditions, we classify these conditions by these two critical parameters (Fig. 4). As mentioned earlier, the oceanic redox condition is classified as OXIC, IWA, and DWA on the basis of the oxygen profiles and as non-sulfidic, IWE, and DWE on the basis of the hydrogen sulfide profiles (Fig. 4a). The standard case is represented by an asterisk in Fig. 4.

The oxidic condition, as might be expected, tends to dominate when the supply flux of oxygen with downwelling water is high because ocean ventilation is active and/or the phosphorus riverine input flux is relatively low (lower right-hand corner of the domain). In particular, anoxia and euxinia will not be achieved with R_p/R_p^* values of less than 0.6 and 1.25, respectively, even when ocean circulation is completely stagnant. In contrast, weakened circulation and/or enhanced riverine input cause eutrophic and productive ocean conditions, generating an

oxygen-depleted water mass (upper left-hand corner). Note that $\langle C_{org}/P_{reactive} \rangle$ and the export production are nearly independent of the ocean circulation rate for any R_p value (Fig. 4b, c) because the phosphorus benthic flux deduced from the occurrence of DWA has a relatively weak effect on the oceanic phosphate budget. As the oxidic–anoxic boundary drifts upward to shallower depths, the $\langle C_{org}/P_{reactive} \rangle$ ratio increases greatly, owing mainly to massive P regeneration and efficient recycling of P from sediments, dramatically changing the oceanic redox environment (Fig. 4b). The required value of R_p/R_p^* for such a drastic change is nearly independent of the ocean circulation rate.

The oxygen budget in the ocean is determined by balance between consumption via oxidation of sinking organic matters and supply via ocean circulation and mixing. Our result indicates that the almost 40 and 80% decreases in oxygen budget from standard case will be required to generate anoxia and euxinia, respectively (Fig. 4d). An increased phosphate inventory in the ocean has been invoked as a necessary condition for widespread anoxia/euxinia (e.g., Hotinski et al., 2001; Meyer and Kump, 2008; Meyer et al., 2008; Misumi and Yamanaka, 2008). Our result indicates that more than four times the amount of phosphate in the standard case will be required to generate euxinia in the ocean (Fig. 4e).

Several lines of evidence suggest that mid-Cretaceous OAEs are linked to extensive volcanism (e.g., Kuroda et al., 2007; Tejada et al., 2009; Turgeon and Creaser, 2008). Our results suggest that continental weathering and enhanced delivery of nutrients from continent to ocean, forced by elevated atmospheric pCO₂ levels, promoted eutrophication and the expansion of the oxygen minimum zone, triggering shallow water anoxia and then global anoxia/euxinia.

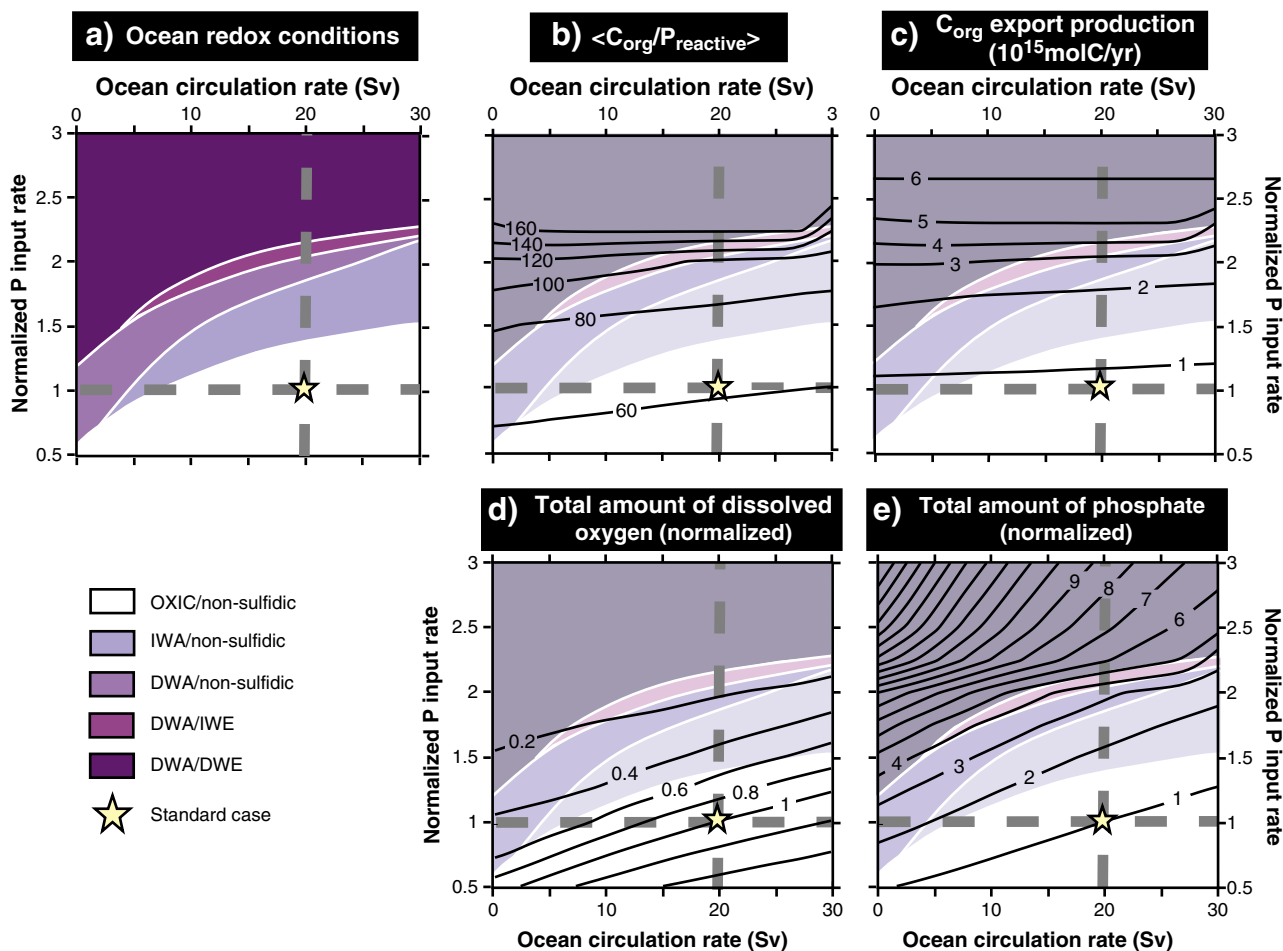


Fig. 4. Oceanic redox conditions with respect to ocean circulation rate and riverine P input flux. (a) Oceanic redox conditions based on oxygen and hydrogen sulfide profiles. OXIC, IWA, and DWA denote fully oxic conditions, intermediate water anoxia, and deepwater anoxia, respectively. Non-sulfidic, IWE, and DWE denote non-sulfidic conditions, intermediate water euxinia, and deepwater euxinia, respectively. (b) $\langle C_{org}/P_{reactive} \rangle$ (= total organic carbon burial rate divided by total reactive P burial rate). (c) Export production of organic carbon (10^{15} mol C/yr). (d) Total amount of dissolved oxygen (normalized) in the ocean. (e) Total amount of phosphate (normalized) in the ocean.

3.4. Effect of oxygen solubility

The dissolved oxygen concentration of surface and downwelling waters might also affect the redox condition of the ocean interior. In the modern oxic ocean, downwelling polar cold waters with a high dissolved oxygen concentration transport oxygen to the intermediate-deep ocean (Broecker and Peng, 1982). At a given partial pressure of O_2 in the atmosphere, the dissolved oxygen content of the mixed layer of the ocean is primarily a function of sea surface temperature (SST). Global warming of the Earth's climate, such as that during the Cretaceous greenhouse world, should decrease oxygen solubility. If the temperature in the deepwater formation region is higher than that at present, and thus the deepwater temperature is also higher, the effect of solubility on the oceanic redox condition could be large.

To assess the effect of decreasing oxygen solubility on the occurrence of anoxia/euxinia, we examined the sensitivity to SST. For simplicity, we assume that the SSTs of the surface layers (M and H) change with the same magnitude. The resulting oxygen, phosphate, and nitrate profiles in steady-state simulations are illustrated in Fig. 5. Clearly, an increase in SST promotes oxygen depletion, but DWA or euxinia is not achieved even when the deviation of SST from the standard value increases to 15 °C.

The conditions for the occurrence of anoxia/euxinia with respect to the change in SST (dSST) vs. R_p/R_p^* and dSST vs. ocean circulation rate are illustrated in Fig. 6. As expected, global warming promotes global anoxia/euxinia because the critical value of R_p/R_p^* decreases (Fig. 6a). However, the decrease in solubility due to global warming cannot

cause OAEs by itself. An enhanced P supply due to increased chemical weathering caused by global warming, combined with the decrease in solubility, may be required for OAEs to occur.

3.5. Role of anoxia-productivity feedback

Finally, we examine the effect of the oxygen dependence of phosphorus burial on oceanic redox conditions. Fig. 7 shows the redox conditions with respect to R_p/R_p^* vs. ocean circulation rate (Fig. 7a), dSST vs. R_p/R_p^* (Fig. 7b), and dSST vs. ocean circulation rate (Fig. 7c) obtained from calculations made without considering the redox-dependent efficiency of P recycling. In these cases, the oceanic C and P cycles are tightly coupled, and the phosphorus burial rate is proportional to the organic carbon burial rate. Thus, export production in the steady state is determined only by the riverine phosphorus input flux. The obtained conditions for ocean anoxia/euxinia are much more restricted than those shown in Figs. 4 and 6. A higher phosphorus input flux and/or weaker ocean circulation rate and/or larger decrease in oxygen solubility are required for anoxia/euxinia to occur. This is because tight coupling of the C and P cycles efficiently removes nutrients from the ocean, preventing ocean eutrophication. Conversely, the redox condition of the ocean is strongly influenced by the decoupling of C and P cycles due to redox-dependency. We therefore conclude that positive feedback among phosphorus regeneration, biological productivity, and anoxia is a critical mechanism for OAE occurrence.

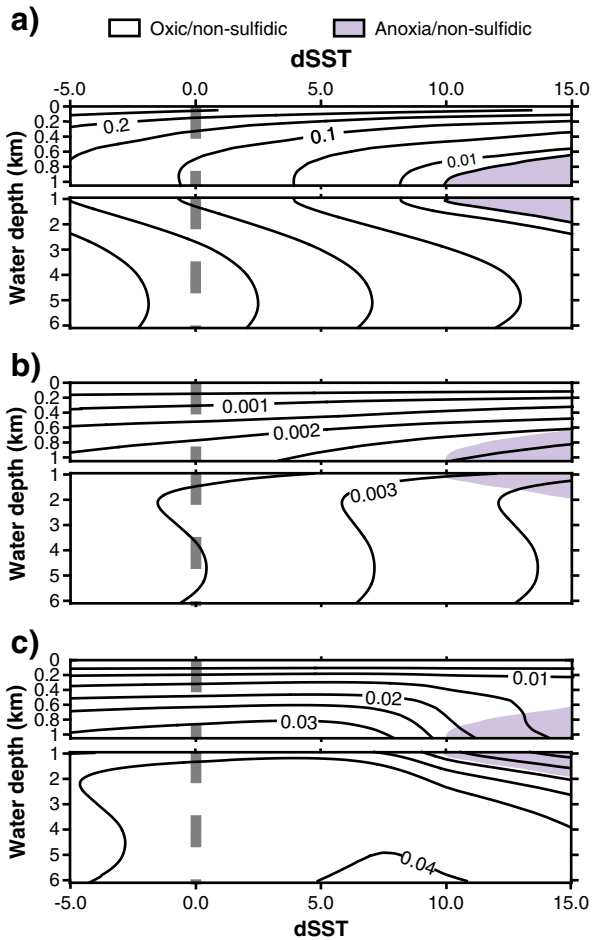


Fig. 5. Effect of SST changes on oceanic redox conditions. Results are obtained for a steady state. Vertical profiles of (a) dissolved oxygen, (b) phosphate, and (c) nitrate concentrations (in mol/m³). Light shading represents anoxic water.

We assumed $(C/P)^a = 1060$ as an upper limit estimated from observations of modern anoxic marine sediments (e.g., Algeo and Ingall, 2007; Slomp and Van Cappellen, 2007). However, the geological records from OAEs sometimes show a larger $(C/P)^a$ signal (e.g., Ingall et al., 1993; Murphy et al., 2000) and also $C_{org}/P_{reactive}$ (e.g., Kraal et al., 2010; Mort et al., 2007). When $(C/P)^a = 4240$ is assumed, the necessary conditions for anoxia/euxinia are moderately reduced;

DWE conditions will appear at $R_p/R_p^* > 2.0$ under the standard ocean circulation rate (compare this with Fig. 3, $R_p/R_p^* > 2.2$). Although further understanding of P cycling in anoxic marine sediments is needed to elucidate the role of anoxia-productivity feedback, we expect the influence of P cycling on the mechanisms of OAEs to be crucial.

4. Conclusions and implications

We developed a new ocean biogeochemical model to systematically examine the proposed causal mechanisms of OAEs. In addition to redox reactions under an oxic environment, the model includes decomposition of organic matter by nitrate and sulfate, reoxidation processes of ammonium and hydrogen sulfide, and the redox-dependent burial efficiency of phosphorus.

We examined oceanic redox states as functions of riverine P input flux, ocean circulation rate, and SST. We found that the marine environment is greatly affected by redox-dependent phosphorus regeneration in marine sediments. Because of this feedback mechanism, the required conditions for anoxia/euxinia are much easier to realize (Figs. 4 and 6). A decrease in oxygen solubility due to global warming and slower circulation also cause anoxia/euxinia much more easily than in the standard case. However, our results indicate that ocean stagnation and/or a rise in SST alone are not enough to achieve global anoxia/euxinia. Shallow water anoxia, which is easily brought about by enhanced riverine P supply, would be a critical mechanism in developing anoxia/euxinia by promoting massive phosphorus liberation from sediments. Our results support the scenario that massive volcanic activity followed by rapid global warming would accelerate weathering on land and nutrient loading to the ocean, probably triggering ocean eutrophication and global anoxia/euxinia.

The appearance of anoxia/euxinia, a subsequent increase in biological productivity, and enhanced organic carbon burial would have played a role in a negative feedback mechanism against an increased level of atmospheric carbon dioxide during Cretaceous OAEs (Kuypers et al., 1999; Sinninghe Damsté et al., 2010; Tajika, 1998). The concentrations of atmospheric CO₂ and O₂ would be strongly influenced by the promotion of phosphorus regeneration in sediments underlying anoxic bottom waters.

However, we should investigate the behavior of phosphorus cycles in the ocean in more detail. Phosphorus burial as an iron-bound phase at the mid-ocean ridge, which is not considered in this study, might have been important for the phosphorus cycle during the Cretaceous. A detailed assessment of benthic nutrient flux by coupling with an early diagenetic model (e.g., Bjerrum et al., 2006; Wallmann, 2003) or

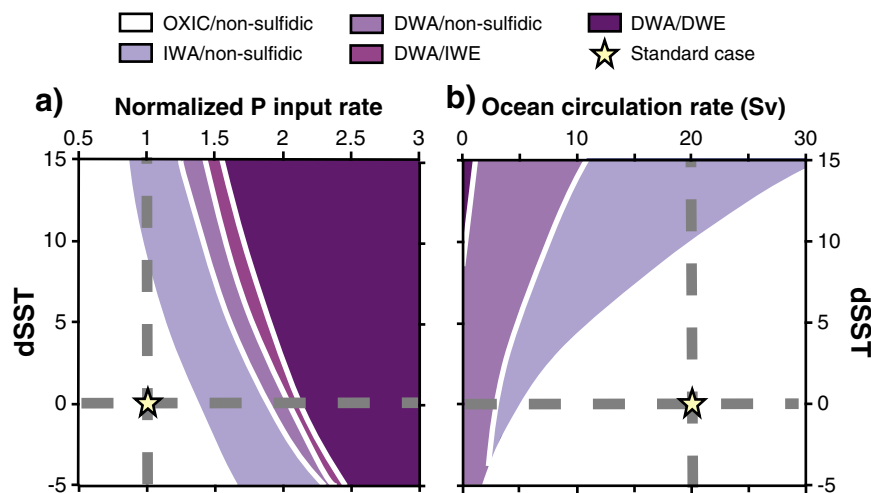


Fig. 6. Oceanic redox conditions over the parameter space of the forcing parameters: (a) dSST and R_p/R_p^* and (b) dSST and ocean circulation rate. Abbreviations have the same meanings as in Fig. 4a.

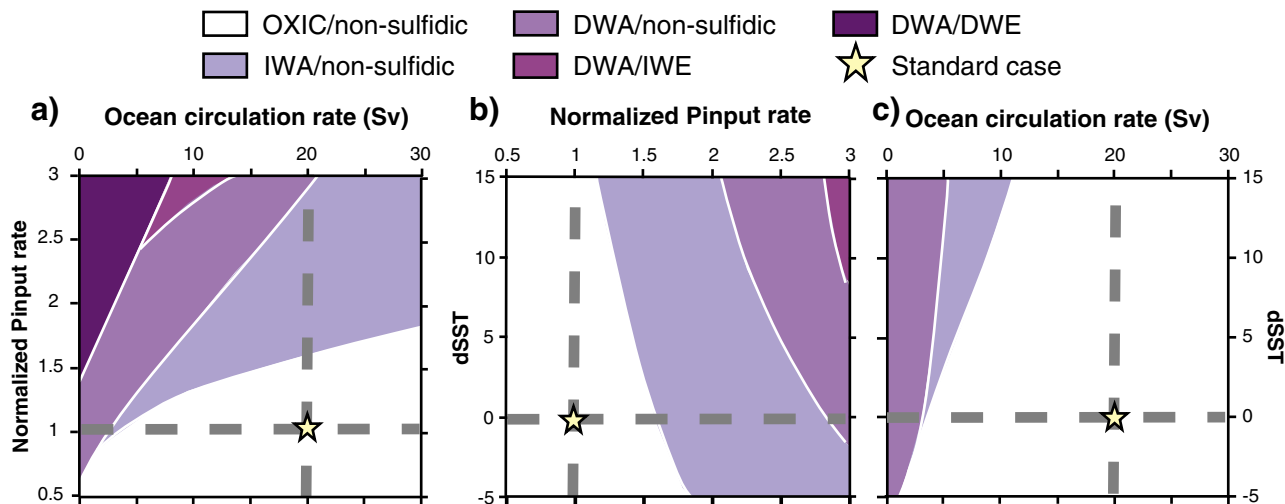


Fig. 7. Oceanic redox conditions without considering the oxygen-dependent P burial process; diagrams for (a) riverine P input flux and ocean circulation rate, (b) SST change and riverine P input flux, and (c) SST change and ocean circulation rate. Abbreviations have the same meanings as in Fig. 4a.

an intermediate- to high-complexity ocean model that includes several redox reactions in anoxic waters (Meyer et al., 2008; Romaniello and Derry, 2010; this study) could provide further insight into reconstruction of the oceanic environment during OAEs.

Acknowledgements

We thank an anonymous reviewer for constructive reviews and comments, and Ryuji Tada, Naohiko Ohkouchi, Junichiro Kuroda, and Yuichiro Kashiya for their insightful comments. This research was partially supported by a Grant-in-Aid for Scientific Research (No. 20340144) of the Japan Society for the Promotion of Science.

References

- Adams, D.D., Hurtgen, M.T., Sageman, B.B., 2010. Volcanic triggering of a biogeochemical cascade during Oceanic Anoxic Event 2. *Nat. Geosci.* 3, 201–204.
- Algeo, T.J., Ingall, E., 2007. Sedimentary Corg:P ratios, paleocean ventilation, and Phanerozoic atmospheric pO₂. *Palaeogeogr. Palaeoclimatol. Palaeoecol.* 256, 130–155.
- Anderson, L.A., Sarmiento, J.L., 1994. Redfield ratios of remineralization determined by nutrient data analysis. *Glob. Biogeochem. Cycles* 8 (1), 65–80.
- Anderson, L.D., Delaney, M.L., Faul, K.L., 2001. Carbon to phosphorus ratios in sediments: implications for nutrient cycling. *Glob. Biogeochem. Cycles* 15 (1), 65–79.
- Arthur, M.A., Sageman, B.B., 1994. Marine black shales: depositional mechanisms and environments of ancient deposits. *Annu. Rev. Earth Planet. Sci.* 22, 499–551.
- Benitez-Nelson, C.R., 2000. The biogeochemical cycling of phosphorus in marine systems. *Earth Sci. Rev.* 51, 109–135.
- Berelson, W.M., 2002. Particle settling rates increase with depth in the ocean. *Deep Sea Res.* 49, 237–251.
- Betts, J.N., Holland, H.D., 1991. The oxygen content of ocean bottom waters, the burial efficiency of organic carbon, and the regulation of atmospheric oxygen. *Palaeogeogr. Palaeoclimatol. Palaeoecol.* 97, 5–18.
- Bjerrum, C.J., Bendtsen, J., Legarth, J.J.F., 2006. Modeling organic carbon burial during sea level rise with reference to the Cretaceous. *Geochem. Geophys. Geosyst.* 7, Q05008. doi:10.1029/2005GC001032.
- Boudreau, B.P., 1996. A method-of-lines code for carbon and nutrient diagenesis in aquatic sediments. *Comput. Geosci.* 22, 479–496.
- Bralower, T.J., Thierstein, H.R., 1984. Low productivity and slow deep-water circulation in mid-Cretaceous oceans. *Geology* 12, 614–618.
- Broecker, W.S., Peng, T.-H., 1982. *Tracers in the Sea*. Eldigio, Palisades, New York.
- Delaney, M.L., 1998. Phosphorus accumulation in marine sediments and the oceanic phosphorus cycle. *Glob. Biogeochem. Cycles* 12 (4), 563–572.
- Erbacher, J., Huber, B.T., Norris, R.D., Markey, M., 2001. Increased thermohaline stratification as a possible cause for an ocean anoxic event in the Cretaceous period. *Nature* 409, 325–327. doi:10.1038/35053041.
- Filippelli, G., 2001. Carbon and phosphorus cycling in anoxic sediments of the Saanich Inlet, British Columbia. *Mar. Geol.* 174, 307–321.
- Froelich, P.N., Klunkhammer, G.P., Bender, M.L., Luedtke, N.A., Heath, G.R., Cullen, D., Dauphin, P., Hammond, D., Hartman, B., Maynard, V., 1979. Early oxidation of organic matter in pelagic sediments of the eastern equatorial Atlantic: suboxic diagenesis. *Geochim. Cosmochim. Acta* 43, 1075–1090.
- Garcia, H., Gordon, L.I., 1992. Oxygen solubility in seawater: better fitting equations. *Limnol. Oceanogr.* 37 (6), 1307–1312.
- Handoh, I.C., Lenton, T.M., 2003. Periodic mid-Cretaceous oceanic anoxic events linked by oscillations of the phosphorus and oxygen biogeochemical cycles. *Glob. Biogeochem. Cycles* 17 (4), 1092. doi:10.1029/2003GB002039.
- Henrichs, S.M., Reeburgh, W.S., 1987. Anaerobic mineralization of marine sediment organic matter: rates and the role of anaerobic processes in the oceanic carbon economy. *Geomicrobiol. J.* 5, 191–237.
- Hensen, C., Landenberger, H., Zabel, M., Schulz, H.D., 1998. Quantification of diffusive benthic fluxes of nitrate, phosphate, and silicate in the southern Atlantic Ocean. *Glob. Biogeochem. Cycles* 12, 193–210.
- Hochuli, P.A., Menegatti, A.P., Weissert, H., Riva, A., Erba, E., Premoli Silva, I., 1999. Episodes of high productivity and cooling in the early Aptian Alpine Tethys. *Geology* 27, 657–660.
- Hotinski, R.M., Kump, L.R., Najjar, R.G., 2000. Opening Pandora's Box: the impact of open system modeling on interpretations of anoxia. *Paleoceanography* 15 (3), 267–279.
- Hotinski, R.M., Bice, K.L., Kump, L.R., Najjar, R.G., Arthur, M.A., 2001. Ocean stagnation and end-Permian anoxia. *Geology* 29, 7–10.
- Ikeda, T., Tajika, E., 2002. Carbon cycling and climate change during the last glacial cycle inferred from the isotope records using an ocean biochemical carbon cycle model. *Glob. Planet. Change* 35, 131–141.
- Ikeda, T., Tajika, E., Tada, R., 2002. Carbon cycle during the last 315,000 years: reconstruction from a marine carbon cycle model. *Glob. Planet. Change* 33, 1–13.
- Ingall, E., Jahnke, R., 1994. Evidence for enhanced phosphorus regeneration from marine sediments overlain by oxygen depleted waters. *Geochim. Cosmochim. Acta* 58 (11), 2571–2575.
- Ingall, E.D., Jahnke, R.A., 1997. Influence of water-column anoxia on the elemental fractionation of carbon and phosphorus during sediment diagenesis. *Mar. Geol.* 139, 219–229.
- Ingall, E.D., Van Cappellen, P., 1990. Relation between sedimentation rate and burial of organic phosphorus and organic carbon in marine sediments. *Geochim. Cosmochim. Acta* 54, 373–386.
- Ingall, E.D., Bustin, R.M., Van Cappellen, P., 1993. Influence of water column anoxia on the burial and preservation of carbon and phosphorus in marine shales. *Geochim. Cosmochim. Acta* 57, 303–316.
- Jenkyns, H.C., 2010. Geochemistry of oceanic anoxic events. *Geochem. Geophys. Geosyst.* 11, Q03004. doi:10.1029/2009GC002788.
- Junium, C.K., Arthur, M.A., 2007. Nitrogen cycling during the Cretaceous, Cenomanian–Turonian Oceanic Anoxic Event 2. *Geochem. Geophys. Geosyst.* 8, Q03002. doi:10.1029/2006GC001328.
- Kashiya, Y., Ogawa, N.O., Kuroda, J., Shiro, M., Nomoto, S., Tada, R., Kitazato, H., Ohkouchi, N., 2008. Diazotrophic cyanobacteria as the major photoautotrophs during mid-Cretaceous oceanic anoxic events: nitrogen and carbon isotopic evidence from sedimentary porphyrin. *Org. Geochem.* 39, 532–549.
- Knox, F., McElroy, M.B., 1984. Changes in atmospheric CO₂: influence of the marine biota at high latitude. *J. Geophys. Res.* 89 (3), 4629–4637.
- Kraal, P., Slomp, C.P., Forster, A., Kuypers, M.M.M., 2010. Phosphorus cycling from the margin to abyssal depths in the proto-Atlantic during oceanic anoxic event 2. *Palaeogeogr. Palaeoclimatol. Palaeoecol.* 295, 42–54.
- Kuroda, J., Ogawa, N.O., Tanimizu, M., Coffin, M.F., Tokuyama, H., Kitazato, H., Ohkouchi, N., 2007. Contemporaneous massive subaerial volcanism and late Cretaceous Oceanic Anoxic Event 2. *Earth Planet. Sci. Lett.* 256, 211–223.
- Kuypers, M.M.M., Pancost, R.D., Sinninghe Damsté, J.S., 1999. A large and abrupt fall in atmospheric CO₂ concentration during Cretaceous times. *Nature* 399, 342–345.

- Kuypers, M.M.M., Pancost, R.D., Nijenhuis, I.A., Sinninghe Damsté, J.S., 2002. Enhanced productivity led to increased organic carbon burial in the euxinic North Atlantic basin during the late Cenomanian oceanic anoxic event. *Paleoceanography* 17 (4), 1051. doi:10.1029/2000PA000569.
- Kuypers, M.M.M., van Breugel, Y., Schouten, S., Erba, E., Sinninghe Damsté, J.S., 2004. N₂-fixing cyanobacteria supplied nutrient N for Cretaceous oceanic anoxic events. *Geology* 32, 853–856.
- Lenton, T.M., 2000. Land and ocean carbon cycle feedback effects on global warming in a simple Earth system model. *Tellus Ser. B* 52, 1159–1188.
- Lenton, T.M., Watson, A.J., 2000. Redfield revisited 1. Regulation of nitrate, phosphate, and oxygen in the ocean. *Glob. Biogeochem. Cycles* 14 (1), 225–248.
- McManus, J., Berelson, W., Coale, K., Johnson, K., Kilgore, T., 1997. Phosphorus regeneration in continental margin sediments. *Geochim. Cosmochim. Acta* 61, 2891–2907.
- Meyer, K.M., Kump, L.R., 2008. Oceanic euxinia in Earth history: causes and consequences. *Annu. Rev. Earth Planet. Sci.* 36, 251–288.
- Meyer, K.M., Kump, L.R., Ridgwell, A., 2008. Biogeochemical controls on photic-zone euxinia during the end-Permian mass extinction. *Geology* 36, 747–750.
- Millero, F.J., 2006. *Chemical Oceanography*, third ed. Taylor & Francis Group CRC Press, p. 496.
- Misumi, K., Yamanaka, Y., 2008. Ocean anoxic events in the mid-Cretaceous simulated by a 3-D biogeochemical general circulation model. *Cretaceous Res.* 29, 893–900.
- Misumi, K., Yamanaka, Y., Tajika, E., 2009. Numerical simulation of atmospheric and oceanic biogeochemical cycles to an episodic CO₂ release event: implications for the causes of mid-Cretaceous Ocean Anoxic Event-1a. *Earth Planet. Sci. Lett.* 286, 316–323.
- Mort, H.P., Adatte, T., Föllmi, K.B., Keller, G., Steinmann, P., Matera, V., Berner, Z., Stüben, D., 2007. Phosphorus and the roles of productivity and nutrient recycling during oceanic anoxic event 2. *Geology* 35, 483–486.
- Mort, H.P., Adatte, T., Keller, G., Bartels, D., Föllmi, K.B., Steinmann, P., Berner, Z., Chellai, E.H., 2008. Organic carbon deposition and phosphorus accumulation during Oceanic Anoxic Event 2 in Tarfaya, Morocco. *Cretaceous Res.* 29, 1008–1023.
- Murphy, A.E., Sageman, B.B., Hollander, D.J., 2000. Eutrophication by decoupling of the marine biogeochemical cycles of C, N, and P: a mechanism for the Late Devonian mass extinction. *Geology* 28, 427–430.
- Nederbragt, A.J., Thurov, J., Vonhof, H., Brumsack, H.-J., 2004. Modelling oceanic carbon and phosphorus fluxes: implications for the cause of the late Cenomanian Oceanic Anoxic Event (OAE2). *J. Geol. Soc. Lond.* 161, 721–728.
- Oguz, T., Murray, J.W., Callahan, A.E., 2001. Modeling redox cycling across the suboxic–anoxic interface zone in the Black Sea. *Deep Sea Res.* 48, 761–787.
- Ohkouchi, N., Kashiyama, Y., Kuroda, J., Ogawa, N.O., Kitazato, H., 2006. The importance of diazotrophic cyanobacteria as primary producers during Cretaceous Oceanic Anoxic Event 2. *Biogeosciences* 3, 467–478.
- Redfield, A.C., Ketchum, B.H., Richards, F.A., 1963. The influence of organisms on the composition of seawater. In: Hill, M.N. (Ed.), *The sea*, v. 2. Interscience.
- Romaniello, S.J., Derry, L.A., 2010. An intermediate-complexity model for simulating marine biogeochemistry in deep time: validation against the modern global ocean. *Geochim. Geophys. Geosyst.* 11, Q08001. doi:10.1029/2009GC002711.
- Ruttenberg, K.C., 1993. Reassessment of the oceanic residence time of phosphorus. *Chem. Geol.* 107, 405–409.
- Ruttenberg, K.C., 2003. The global phosphorus cycle. In: Schlesinger, W.H. (Ed.), *Treatise on Geochemistry*, vol 8. Elsevier, USA, pp. 585–643.
- Ruttenberg, K.C., Berner, R.A., 1993. Authigenic apatite formation and burial in sediments from non-upwelling, continental margin environments. *Geochim. Cosmochim. Acta* 57, 991–1007.
- Sarmiento, J.L., Herbert, T.D., Toggweiler, J.R., 1988. Causes of anoxia in the world ocean. *Glob. Biogeochem. Cycles* 2 (2), 115–128.
- Schlanger, S.O., Jenkyns, H.C., 1976. Cretaceous oceanic anoxic events: causes and consequences. *Geol. Mijnb.* 55, 179–184.
- Shaffer, G., 1989. A model of biogeochemical cycling of phosphorus, nitrogen, oxygen, and sulphur in the ocean: one step toward a global climate model. *J. Geophys. Res.* 94, 1979–2004.
- Shaffer, G., 1996. Biogeochemical cycling in the global ocean 2. New production, Redfield ratios, and remineralization in the organic pump. *J. Geophys. Res.* 101, 3723–3745.
- Shaffer, G., Sarmiento, J.L., 1995. Biogeochemical cycling in the global ocean 1. A new, analytical model with continuous vertical resolution and high-latitude dynamics. *J. Geophys. Res.* 100, 2659–2672.
- Sinninghe Damsté, J.S., van Bentum, E.C., Reichert, G., Pross, J., Schouten, S., 2010. A CO₂ decrease-driven cooling and increased latitudinal temperature gradient during the mid-Cretaceous Oceanic Anoxic Event 2. *Earth Planet. Sci. Lett.* 293, 97–103.
- Slomp, C.P., Van Cappellen, P., 2007. The global marine phosphorus cycle: sensitivity to oceanic circulation. *Biogeosciences* 4, 155–171.
- Slomp, C.P., Thomson, J., de Lange, G.J., 2002. Enhanced regeneration of phosphorus during formation of the most recent eastern Mediterranean sapropel (S1). *Geochim. Cosmochim. Acta* 66 (7), 1171–1184.
- Suess, E., 1980. Particulate organic carbon flux in the oceans–surface productivity and oxygen utilization. *Nature* 288, 260–263.
- Tajika, E., 1998. Climate change during the last 150 million years: reconstruction from a carbon cycle model. *Earth Planet. Sci. Lett.* 160, 695–707.
- Tejada, M.L.G., Suzuki, K., Kuroda, J., Coccioni, R., Mahoney, J.J., Ohkouchi, N., Sakamoto, T., Tatsumi, Y., 2009. Ontong Java Plateau eruption as a trigger for the early Aptian oceanic anoxic event. *Geology* 37, 855–858.
- Tromp, T.K., Van Cappellen, P., Key, R.M., 1995. A global model for the early diagenesis of organic carbon and organic phosphorus in marine sediments. *Geochim. Cosmochim. Acta* 59, 1259–1284.
- Tsandeov, I., Slomp, C.P., 2009. Modeling phosphorus cycling and carbon burial during Cretaceous Oceanic Anoxic Events. *Earth Planet. Sci. Lett.* 286, 71–79.
- Turgeon, S.C., Creaser, R.A., 2008. Cretaceous oceanic anoxic event 2 triggered by a massive magmatic episode. *Nature* 454, 323–327.
- Tyrell, T., 1999. The relative influences of nitrogen and phosphorus on oceanic primary production. *Nature* 400, 525–531. doi:10.1038/22941.
- Van Cappellen, P., Ingall, E.D., 1994. Benthic phosphorus regeneration, net primary production, and ocean anoxia: a model of the coupled marine biogeochemical cycles of carbon and phosphorus. *Paleoceanography* 9 (5), 677–692.
- Van Cappellen, P., Ingall, E.D., 1996. Redox stabilization of the atmosphere and oceans by phosphorus-limited marine productivity. *Science* 271, 493–496.
- Van Cappellen, P., Wang, Y., 1996. Cycling of iron and manganese in surface sediments: a general theory for the coupled transport and reaction of carbon, oxygen, nitrogen, sulfur, iron and manganese. *Am. J. Sci.* 296, 197–243.
- Wallmann, K., 2003. Feedbacks between oceanic redox states and marine productivity: a model perspective focused on benthic phosphorus cycling. *Global Biogeochem. Cycles*, 17, 3, p. 1084. doi:10.1029/2002GB001968.
- Wortmann, U.G., Chernyavsky, B.M., 2007. Effect of evaporite deposition on Early Cretaceous carbon and sulphur cycling. *Nature* 446, 654–656. doi:10.1038/05693.
- Yamanaka, Y., Tajika, E., 1996. The role of the vertical fluxes of particulate organic matter and calcite in the oceanic carbon cycle: studies using an ocean biogeochemical general circulation model. *Glob. Biogeochem. Cycles* 10, 361–382.